

Dmitry Kolomenskiy · Henry Keith Moffatt · Marie Farge ·
Kai Schneider

Vorticity generation during the clap–fling–sweep of some hovering insects

Received: 13 November 2008 / Accepted: 2 July 2009
© Springer-Verlag 2009

Abstract Numerical simulations of the Lighthill–Weis-Fogh mechanism are performed using a Fourier pseudo-spectral method with volume penalization. Single-winged and double-winged configurations are compared, and the vortex shedding patterns are related to the lift generated in both cases. The computations of the lift coefficient are validated against the results reported previously by Miller and Peskin (J Exp Biol 208:195–212, 2005).

Keywords Lighthill–Weis-Fogh mechanism · Insect flight · Vortex flows · Volume penalization method

PACS 47.63.-b, 47.63.M-

1 Introduction

The Lighthill–Weis-Fogh clap–fling–sweep mechanism is a movement of wings used by some insects to improve their flight performance. In 1973 Weis-Fogh [1] studied the flight of different hovering insects, such as some species of moths, flies or wasps, in particular the Chalcid wasp *Encarsia formosa* whose wing span is less than 2 mm. It has two pairs of wings, with a wing chord of about 0.2 mm, which move as a single unit. Weis-Fogh showed that the observed lift coefficient is much too high to be compatible with steady-state aerodynamics and, by taking movies at frequency 7150 s^{-1} , he decomposed each downstroke, whose frequency is about 400 s^{-1} , into three phases: the wings clap at the end of upstroke, ‘fling open’ like a book, then separate and sweep horizontally until the end of downstroke. Although the motion is three-dimensional, Lighthill showed the same year [2] that the lift generation can be explained using only two-dimensional inviscid fluid dynamics.

Communicated by H. Aref

D. Kolomenskiy (✉)
M2P2-CNRS, Universités d’Aix-Marseille, 38 rue Joliot-Curie, 13451 Marseille Cedex 20, France
E-mail: dkolom@L3m.univ-mrs.fr

H. K. Moffatt
Department of Applied Mathematics and Theoretical Physics, Centre for Mathematical Sciences,
University of Cambridge, Wilberforce Road, Cambridge CB3 0WA, UK
E-mail: H.K.Moffatt@damtp.cam.ac.uk

M. Farge
LMD-IPSL-CNRS, Ecole Normale Supérieure, 24 rue Lhomond, 75231 Paris Cedex 5, France
E-mail: farge@lmd.ens.fr

K. Schneider
M2P2-CNRS and CMI, Universités d’Aix-Marseille, 39 rue Joliot-Curie, 13453 Marseille Cedex 13, France
E-mail: kschneid@cmi.univ-mrs.fr

We propose to consider Lighthill's two-dimensional model, but using instead viscous fluid dynamics to study how such an unsteady motion generates vorticity, circulation, and lift on the wings. Numerical solution of the Navier–Stokes equations gives us an insight into both the vortex dynamics and the lift generation. In addition, we make a comparison of our results with those obtained by Miller and Peskin [3] using a different numerical method.

2 Fluid–structure interaction model

The fluid–structure interaction model used in this work is an extension of the one described in [4,5] to the case of two symmetrically moving wings. We consider solid obstacles, e.g., wings, placed in a viscous incompressible fluid. The motion of the fluid is governed by the Navier–Stokes equations, completed with a no-slip condition at the solid–fluid interface and a suitable initial condition. The flow is two-dimensional, therefore we use the vorticity-stream function formulation of the equations. The no-slip boundary condition is modelled using the volume penalization method [6]. The wings are assumed to be slightly permeable, and the flow is governed by the penalized equation

$$\partial_t \omega_\eta + \mathbf{u}_\eta \cdot \nabla \omega_\eta - \nu \nabla^2 \omega_\eta + \nabla \times \left(\frac{\chi}{\eta} (\mathbf{u}_\eta - \mathbf{u}_s) \right) = 0, \quad (1)$$

where the penalization parameter η is a small number which controls the permeability of the obstacle. The equation is written for dimensionless parameters and variables. Units are chosen in order to set the dimensionless density $\rho = 1$. The vorticity ω_η is unknown. The velocity is determined as a sum $\mathbf{u}_\eta = \nabla^\perp \Psi + \mathbf{U}_\infty$, with \mathbf{U}_∞ being the free-stream velocity and Ψ being the stream function, satisfying

$$\nabla^2 \Psi = \omega_\eta, \quad (2)$$

where $\nabla^\perp \Psi = (-\partial_y \Psi, \partial_x \Psi)$ stands for the orthogonal gradient of the stream function. The parameter ν is the kinematic viscosity. Equations (1) and (2) are valid in a computational domain A which incorporates both the solid wings A_s and the fluid A_f (see Fig. 1). Geometry and kinematics of the wings are given by the mask function

$$\chi = \begin{cases} 1 & \text{for } \mathbf{x} \in A_s \\ 0 & \text{for } \mathbf{x} \in A_f \end{cases} \quad (3)$$

and the velocities of the wings $\mathbf{u}_s(\mathbf{x}, t)$ at each point. The penalized flow field converges towards the no-slip boundary flow field when the penalization parameter η tends to zero [6].

For the spatial discretization of (1) and (2) we use a classical Fourier pseudo-spectral method in a periodic domain A [7]. The vorticity field is dealiased at each time step using the 2/3 rule. The solution is advanced in

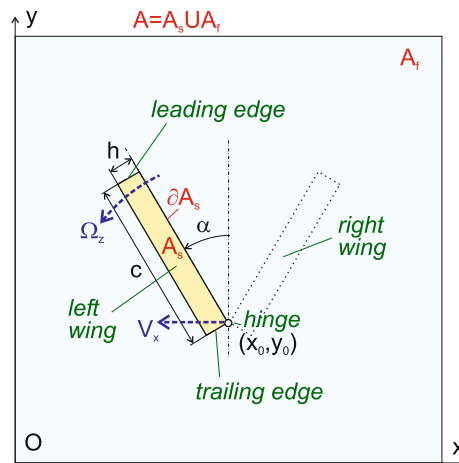


Fig. 1 Sketch of the flapping wing configuration

time with an adaptive second-order Adams–Bashforth scheme for the non-linear term, while the viscous term is integrated exactly.

An attractive feature of the volume penalization method is that it offers the possibility of moving solid obstacles while keeping unchanged the computational mesh. This motion implies changing in time the mask function $\chi(\mathbf{x}, t)$. Translation of the obstacle in each direction is implemented by turning the phase of the corresponding Fourier coefficients, and rotation is decomposed into three skewing operations [5].

The volume penalization method also enables us to compute the fluid forces acting on the wing via volume integration, which is convenient for numerical implementation:

$$\mathbf{F} = \int_A \frac{\chi}{\eta} (\mathbf{u}_\eta - \mathbf{u}_s) dA + V_c \dot{\mathbf{u}}_c, \quad (4)$$

where V_c is the volume of the wing, and $\dot{\mathbf{u}}_c$ is the acceleration of its center of gravity (assuming that its density is uniform).

3 Numerical experiment

3.1 Physical and numerical parameters

Two configurations are considered: *double-winged* and *single-winged*. The single-winged configuration consists of a rectangular wing of chord $c = 1$ and thickness $h = 1/32$. The wing is hinged at its lower-right corner (x_0, y_0) , as shown in Fig. 1.

We decompose the flapping motion into three phases. *Clap*: at time $t = 0$ the wing is arranged vertically. *Fling*: it starts rotating with a linearly increasing angular velocity Ω_z . At time $t = 0.1$ the angular velocity mounts to its maximum $\Omega_z = \Omega_{\max} = 4$ and then starts decreasing as $\Omega_z = \Omega_{\max} \exp(-15.5[t - 0.1]^2)$. *Sweep*: at $t = 0.275$, when the angle of incidence mounts to approximately $\alpha = 57^\circ$, the wing starts translating in the negative- x direction. The velocity is changing as $V_x = V_{\max} (\exp(-100[t - 0.275]^2) - 1)$, and we consider two cases: $V_{\max} = 1$ and $V_{\max} = 4$. The smooth transient between fling and sweep is introduced to avoid high accelerations and associated added mass effects. Figure 2 displays these kinematics. It shows x —the horizontal coordinate of the hinge, V_x —horizontal component of its velocity, α —angle of the wing, measured between the vertical and the chord, and Ω_z —its angular velocity.

The double-winged configuration has its *left wing* identical to the single-winged configuration, and its *right wing* symmetric with respect to the vertical. The hinge points coincide during the fling phase, such that initially there is no gap between the wings.

The surrounding fluid is initially at rest. Its dimensionless density is $\rho = 1$ and its dimensionless kinematic viscosity is $\nu = 0.05$. These parameters yield dimensionless numbers which are in agreement with what can be observed in nature. Thus, the Reynolds number is $Re_{\text{fling}} = 80$, when based on the chord and the maximum

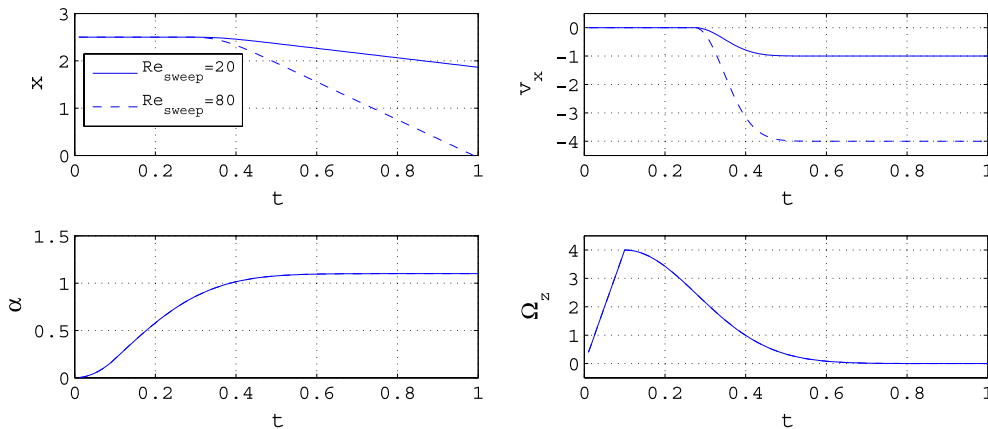


Fig. 2 Kinematics of the flapping motion: horizontal position of the hinge (*top-left*), horizontal velocity (*top-right*), angle of incidence (*bottom-left*), and angular velocity (*bottom-right*) of the left wing

tip-speed during fling, and $Re_{\text{sweep}} = 20$ or 80 , when based on the chord and the translation speed V_{max} during sweep.

The periodic domain is $A = [0, 5] \times [0, 5]$. It is discretized with $N_x \times N_y = 1024 \times 1024$ grid points, which yields 204.8 points per chord and 6.4 points per thickness. The edge of the wing is smoothed with a transitional ‘porous’ layer covering two points inside and two points outside, which models the hairs covering *Encarsia formosa*. The penalization parameter is $\eta = 5 \cdot 10^{-4}$.

3.2 Results

Figure 3 (left) shows the vorticity plots of the *double-winged* configuration at three successive time instants. We observe that strong vortices are formed at the tips of the wings (leading edges), reflecting the fact that the air rushes in the opening. But during sweep these vortices form a pair which remains localized between the wings, generating a downward jet which is not observed for the single wing, see Fig. 3 (right). Another important feature is that the trailing-edge vortices, formed when the wings separate, are of the same sign as the leading-edge vortices, in contrast to [3], which followed a slightly different scenario. This increases the downward air flow through the opening gap, supporting Lighthill’s idea of high lift generation, and showing how the circulation persists during the sweep phase.

Figure 3 (right) presents vorticity plots for the *single wing* following the same protocol. Comparison with Fig. 3 (left) shows the importance of the topology change involved in sweep. Overall, the single-winged configuration exhibits a typical unsteady airfoil flow, which is radically different from the flow generated by the *clap-fling-sweep* mechanism where topology is changing.

Figure 4 shows the time evolution of the lift coefficient produced by both configurations, $c_L = 2F_L / \rho \Omega^2 c^3$, where F_L is the lift force. Only the force acting on the left wing is shown for the double-winged configuration. The latter creates at least double the lift per wing during the fling motion. When the wing stops rotating the

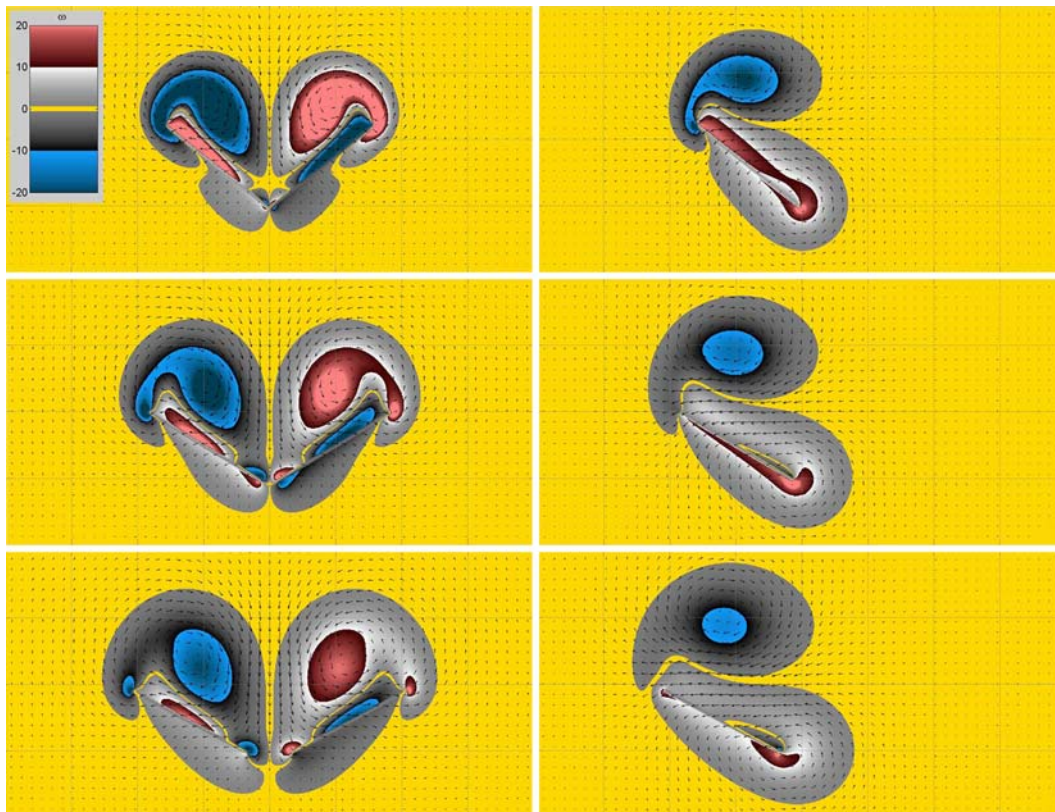


Fig. 3 Vorticity plots of the double-winged (*left*) and the single-winged (*right*) configurations, combined with vector plots of the velocity. Snapshots correspond to the sweep motion at times $t = 0.32$ (*top*), 0.42 (*middle*) and 0.52 (*bottom*)

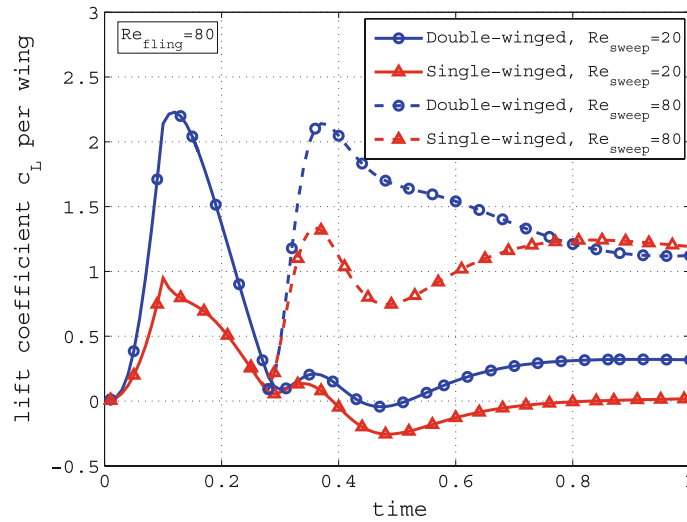


Fig. 4 Lift coefficient per wing of the double-winged and the single-winged configurations

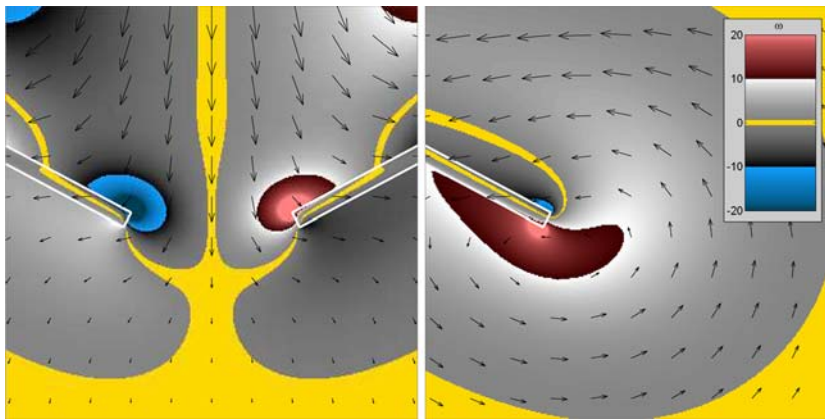


Fig. 5 Flow in the neighbourhood of the trailing edges of the double-winged (*left*) and the single-winged (*right*) configurations at $t = 0.52$

lift drops rapidly for both configurations, which is an added mass effect. The lift recovers after the transition and becomes higher again for the double-winged configuration than for the single-winged. At this stage the difference of the lift coefficient Δc_L is approximately proportional to $(\Gamma_2 - \Gamma_1)V$, where Γ_1 is the circulation around *the wing and its free vortices* for the single-winged configuration, Γ_2 is the circulation corresponding to one wing of the double-winged configuration, and V is the velocity of the hinge. The positive Δc_L supports the idea that the high circulation, created during the fling of the two wings, survives after the change of topology and results in an instantaneous lift. The strength and the sign of the separated vortices are, indeed, crucial for the lift generation at the beginning of sweep (cf. [2,8]).

The leading edge vortices, when they are near to the wing surface, increase the circulation and the lift. In case of the single-winged configuration this is counteracted by the upward flow past the trailing edge (see Fig. 5, which shows a zoom on this region). The situation is different for the double-winged configuration, since the flow field in the neighbourhood of the hinge is due to the action of two mechanisms: (1) a downward jet of the two leading edge vortices, and (2) local low Reynolds number effects, since $Re_{\text{local}} = (r/c)^2 Re_{\text{fling}}$ is tending to zero in the vicinity of the hinge, i.e. for vanishing radii r . The straight iso-vorticity lines radiating from the hinge point, which can be observed in Fig. 3 (left-top), are characteristic for the low Re flow. Therefore local solutions of the Stokes equation derived in [9] are applicable. Both of the above mechanisms result in a negative pressure jump across the hinge, which acts to suppress the possible upflow through the opening between the wings during the initiation of sweep. A more precise analysis of this phenomenon, and especially the low Re effects, will be reported in another paper.

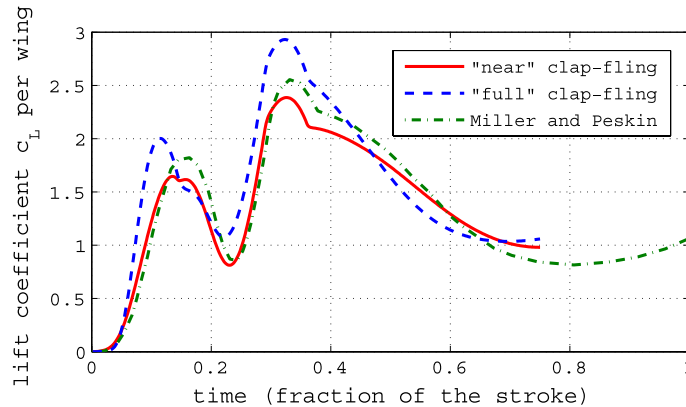


Fig. 6 Comparison of the lift coefficient obtained in the present simulations (*solid and dashed lines*) with the corresponding curve in [3] (*dash-dot*). The spacing between the wing centerlines equals $c/6$ during the ‘near’ clap–fling. During the ‘full’ clap–fling there is no spacing between the wings

4 Comparison with the results of Miller and Peskin

Numerical simulations of the Lighthill–Weis-Fogh mechanism were recently performed by Miller and Peskin [3], who studied influence of the Reynolds number on the lift coefficient. They also compared the single and the double wings. However, they actually considered a so-called ‘near’ clap–fling, since the wings remained separated by a distance of $1/6$ chord length (possibly due to restrictions of the numerical method). Therefore the downward jet between the separating wings is not present in their simulations. They also report a smaller increase in lift, compared to our result shown in Sect. 3.

For the purpose of validation we have applied the fluid–structure interaction code, presented in Sect. 2, to a similar configuration at $Re = 128$, with the same kinematic parameters as described in [3]. The wings are rectangular, their thickness to chord ratio is $1/32$. Unlike in our previous simulations, the hinges are situated at the centerlines of the wings, and not at their corners. This is more consistent with the model of Miller and Peskin, which is based on the immersed boundary method.

The periodic domain size is $L_x \times L_y = 10 \times 10$, it is discretized with $N_x \times N_y = 2048 \times 2048$ grid points. The permeability parameter is $\eta = 5 \cdot 10^{-4}$. Five point smoothing of the mask function is applied. The result of this simulation is shown in a solid line in Fig. 6. The lift coefficient is calculated as $c_L = 2F_L/\rho V^2 c$, where $V = 1.108\Omega_{\max}c$, Ω_{\max} is the maximum angular velocity during fling. The reference curve is shown in dash-dot.

Time is shown as a fraction of the stroke τ/τ_{\max} . Both simulations predict qualitatively the same evolution of the lift coefficient. The discrepancy is of order 10% or less. It can be explained as follows: in [3] theoretically the wings are thin, and the gap ($c/6$) between them is the gap between their centerlines; however in practice the regularized delta function has a support of several grid cells, and the effective gap between the wings becomes smaller, yielding higher lift.

To check the influence of spacing between the wings, or in other words, the difference between the ‘near’ and the ‘full’ clap–fling, we also performed a computation with initially zero spacing between the hinge points. The result is shown in a dashed line in Fig. 6, and it displays 15% higher lift peaks. Note the significant increase in lift during the initial portion of sweep, which is due to stronger vorticity generation in the preceding fling motion. However, the lift drops more rapidly as the wings move further apart.

5 Conclusions

A numerical method has been developed for simulations of solid obstacles moving through a viscous incompressible fluid. It is reasonably efficient, easy to implement and to use even when the topology of the obstacles is changing in time, as in the case of the clap–fling–sweep mechanism where the two wings break apart. The model has been validated against the results reported in [3].

The Lighthill–Weis-Fogh clap–fling–sweep mechanism has been studied. Our numerical simulations confirm that the clap–fling–sweep mechanism enhances the lift, as a consequence of higher circulation round each wing. For the latter, flow in the neighbourhood of the hinge point is of major importance, and its more detailed analysis is envisaged.

Acknowledgments DK, KS and MF acknowledge Trinity College, Cambridge, for hospitality. DK thanks Tony Maxworthy and Jane Wang for useful discussions. Some of the numerical simulations presented in this paper were conducted using NEC SX-8 computer at IDRIS. DK and KS thank the Deutsch-Französische Hochschule, project ‘S-GRK-ED-04-05’, for financial support.

References

1. Weis-Fogh, T.: Quick estimates of flight fitness in hovering animals, including novel mechanisms for lift production. *J. Exp. Biol.* **59**, 169–230 (1973)
2. Lighthill, M.J.: On the Weis-Fogh mechanism of lift generation. *J. Fluid Mech.* **60**(1), 1–17 (1973)
3. Miller, L.A., Peskin, C.S.: A computational fluid dynamics of ‘clap and fling’ in the smallest insects. *J. Exp. Biol.* **208**, 195–212 (2005)
4. Schneider, K., Farge, M.: Numerical simulation of the transient flow behaviour in tube bundles using a volume penalization method. *J. Fluids Struct.* **20**, 555–566 (2005)
5. Kolomenskiy, D., Schneider, K.: A Fourier spectral method for the Navier–Stokes equations with volume penalization for moving solid obstacles. *J. Comput. Phys.* **228**, 5687–5709 (2009)
6. Angot, P., Bruneau, C.H., Fabrie, P.: A penalisation method to take into account obstacles in viscous flows. *Numer. Math.* **81**, 497–520 (1999)
7. Canuto, C., Hussaini, M.Y., Quarteroni, A., Zang, T.A.: *Spectral Methods in Fluid Dynamics*. Springer, New York (1988)
8. Maxworthy, T.: Experiments on the Weis-Fogh mechanism of lift generation by insects in hovering flight. Part 1. Dynamics of the ‘fling’. *J. Fluid Mech.* **93**(1), 47–63 (1979)
9. Moffatt, H.K.: Viscous and resistive eddies near a sharp corner. *J. Fluid Mech.* **18**(1), 1–18 (1963)